Evaluation of Colloids and Activation Agents for Determination of Melamine Using UV-SERS

Evelyn Kämmer,[†,§,⊥] Thomas Dörfer,[†,§,⊥] Andrea Csáki,[§] Wilm Schumacher,[†]
Paulo Augusto Da Costa Filho,[‡] Nicolae Tarcea,[†] Wolfgang Fritzsche,[§] Petra Rösch,[†] Michael Schmitt,[†]
and Jürgen Popp*,[†,§]

[†]Institute of Physical Chemistry and Abbe Center of Photonics, Friedrich Schiller University, Helmholtzweg 4, D-07743 Jena, Germany

[‡]Quality and Safety Department, Nestlé Research Center, Vers-Chez-Les-Blanc, 1000 Lausanne 26, Switzerland

[§]Institute of Photonic Technology, Albert-Einstein-Strasse 9, 07745 Jena, Germany

Ⓢ *Supporting Information*

ABSTRACT: UV-SERS measurements offer a great potential for environmental or food (detection of food contaminats) analytics. Here, the UV-SERS enhancement potential of various kinds of metal colloids, such as Pd, Pt, Au, Ag, Au–Ag core–shell, and Ag–Au core–shell with different shapes and sizes, were studied using melamine as a test molecule. The influence of different activation (KF, KCl, KBr, K_2SO_4) agents onto the SERS activity of the nanomaterials was investigated, showing that the combination of a particular nanoparticle with a special activation agent is extremely crucial for the observed SERS enhancement. In particular, the size dependence of spherical nanoparticles of one particular metal on the activator has been exploited. By doing so, it could be shown that the SERS enhancement increases or decreases for increasing or decreasing size of a nanoparticle, respectively. Overall, the presented results demonstrate the necessity to adjust the nanoparticle size and the activation agent for different experiments in order to achieve the best possible UV-SERS results.
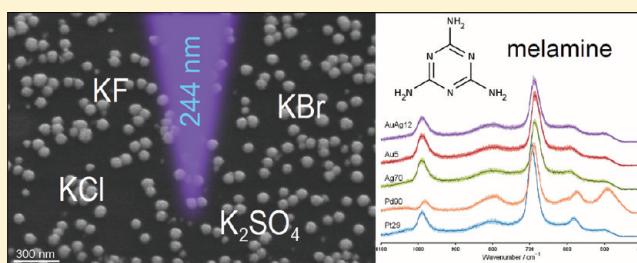
1. INTRODUCTION

In the past decade, surface-enhanced Raman spectroscopy (SERS) has been intensively studied and a wide range of different application fields were developed,[1−6] and also theoretical considerations are upcoming.[7,8] Thereby, an important issue was the optimal SERS excitation wavelength. Until now, mainly the visible range of the electromagnetic spectrum was explored because of the large number of available laser sources in this range, whereas only a few studies report about the application of ultraviolet (UV) excitation wavelengths.[9−15] However, the application of shorter wavelengths for Raman spectroscopy offers several advantages, such as, for example, higher spatial resolution and potentially additional information about the analyte molecule due to electronic resonant excitation. Furthermore, the application of excitation wavelengths in the deep UV very often avoids disturbing fluorescence emission since most molecules do not show fluorescence below 250 nm.[9] In addition, because of the ω^4 dependency of the intensity of the Raman scattered light, the application of UV excitation lines increases the Raman scattering significantly as compared with vis excitation wavelengths. However, the choice of the SERS excitation wavelength depends on the SERS-active material in a way that the excitation wavelength should be in resonance with the plasmon resonance of the used metal nanoparticles. For UV-SERS,

several transition metals, such as platinum (Pt)[16] and palladium (Pd)[17−19] and also aluminum (Al),[20] can be used.

Initially, transition-metal electrodes coated with a variety of different adsorbates were used for UV-SERS. Thus, for example, palladium electrodes were used to investigate pyridine[21] or gold electrodes were applied for the analysis of thymine.[15] Furthermore, several organic molecules were studied by means of UV-SERS, such as, for example, *para*-nitrobenzoic acid in combination with a gold electrode.[13] The potential of copper colloids as a UV-SERS substrate has been evaluated using *para*-hydroxybenzoic acid as a test molecule and 325 nm as the excitation wavelength.[22] Platinum colloids capped with poly(*N*-vinylpyrrolidone) (PVP), in analogy to an absorbate on an electrode, can be also used for UV-SERS experiments.[19] In addition, Pt colloids of various shapes and sizes and in combination with gold as core–shell particles were used as colloidal SERS substrates for the detection of the thiocyanate ion (SCN⁻) and adenine.[16] As already mentioned further above, the application of UV–Raman excitation very often results in electronic resonant Raman excitation since most molecules exhibit an electronic transition in the UV region.

Thus, UV-SERS is very often combined with resonance Raman spectroscopy, which is referred to as UV-SERRS (surface-enhanced resonance Raman spectroscopy). SERRS shows an increased sensitivity as compared with SERS due to the additional resonance Raman enhancement.

For the here presented UV-SERS (or UV-SERRS) studies, we have chosen melamine, which shows an absorption in the deep UV around 200 nm, as a test substance. Melamine (1,3,5-triazine-2,4,6-triamine) is an organic base with a stable heterocyclic structure, and its commercial main application is the production of melamine resins by polycondensation with formaldehyde. Recently, melamine has been used as an adulterant in pet and dairy food products.[23,24] The objective of this adulteration was to simulate a higher protein content by elevating the total nitrogen content detected by some simple protein tests as Kjeldahl analysis, which is the historical reference method for determination of the protein content.[25] The ingestion of melamine can induce the formation of kidney stones and, as a consequence, can even lead to a necrosis and death, as several studies have confirmed.[26−28]

Thus, analytical approaches, with which a selective and also sensitive detection of melamine in food is possible, are required. For analysis of melamine techniques, such as liquid chromatography with electrospray ionization tandem mass spectroscopy and chromatographic methods, such as HPLC-UV, GC-MS, and LC-MS/MS, and also ELISA,[29,30] are used. All these methods show a good performance in detecting melamine. With SERS, the detection of melamine is quite easy and really fast.[31] Also, SERS is highly sensitive and, therefore, very suitable for the analysis of melamine.[32,33] However, the most important issue in SERS investigations is the availability of appropiate SERS substrates leading to large Raman signal enhancement factors together with a high reproducibility. UV-SE(R)RS might be such an analytical approach.

Therefore, the work presented in the following investigates the application of metallic nanoparticles as potential SERS substrates to detect melamine. In particular, we applied Pt, Pd, Au, and Ag nanoparticles as well as Au/Ag core−shell particles. These SERS substrates were characterized by scanning electron microscopy (SEM) or transmission electron microscopy (TEM) and UV−vis absorption spectroscopy. For the UV-SERS experiments, an excitation wavelength of 244 nm has been chosen. In particular, the influence of various activation agents on the nanoparticles' SERS acitivity has been evaluated.

2. EXPERIMENTAL SECTION

2.1. Chemicals and Sample Preparation.
Melamine with a purity of 99.0% was purchased from Sigma Aldrich. For the SERS experiments, a 0.01 M aqueous melamine solution was prepared. As activators for the colloids, different potassium salts, such as potassium chloride (KCl, Fluka, ≥99.5%), potassium fluoride (KF, Roth, ≥99%), and potassium bromide (KBr, Sigma Aldrich, ≥99%), in the form of a 1 M aqueous solution were used. Furthermore, a 0.5 M aqueous potassium sulfate (K_2SO_4, Merck, ≥99%) solution was used for activation because of the reduced water solubility of this salt.

The silver colloids (Ag) with diameters of 23 and 70 nm and the gold colloids (Au) with diameters of 35 and 120 nm were prepared according to the method of Turkevich et al.[34] and Frens.[35] The Ag prisms with different sizes (Table 1) were produced according to Aherne et al.[36] The 5 nm Au particles were prepared by the instructions of Brust et al.[37] All used core−shell particles (AuAg core diameters, 12 and 30 nm;

Table 1. Sizes and Shapes of All Used Colloids, Including the Global and, if Existent, Local UV−vis Absorpion Maxima

	colloid			UV−vis λ_{Max}	
metal	size	shape	abbreviation	global (nm)	local (nm)
palladium	20 nm	spherical	Pd20	247	
palladium	90 nm	spherical	Pd90	280	
platinum	29 nm	spherical	Pt29	200	
platinum	48 nm	spherical	Pt48	200	
platinum	73 nm	spherical	Pt73	200	
platinum	107 nm	spherical	Pt107	200	
gold	5 nm	spherical	Au5	330	
gold	35 nm	spherical	Au35	255	530
gold	120 nm	spherical	Au120	570	300
silver	23 nm	spherical	Ag23	410	
silver	70 nm	spherical	Ag70	435	
silver	edge length 50 nm	prism	Ag50	520	400
silver	edge length 100 nm	prism	Ag100	635	400
silver	edge length 125 nm	prism	Ag125	720	400
silver	edge length 225 nm	prism	Ag225	560	400
core−shell	Au core 12 nm + Ag shell	spherical	AuAg12	420	300
core−shell	Au core 30 nm + Ag shell	spherical	AuAg30	505	250
core−shell	Ag core 25 nm + Au shell	spherical	AgAu25	435	

AgAu core diameter, 25 nm) were assembled by the method of Steinbrück et al.[38] All used palladium (Pd) nanoparticles were made according to Panigrahi et al.,[39] where we modified the ratio between the reducing agent and Pd salts from 1:1 for the 20 nm particles to 1:4 to obtain 90 nm Pd colloids. To prepare the respective Pd colloids, 1 mL of the Pd particle suspension was applied in 9 mL of distilled water. All platinum (Pt) particles were obtained using the instructions of Bigall et al.[40] Table 1 summarizes all nanoparticles applied within this study.

The ratio of analyte to colloid to activator was 1:1:0.1 in relation to the total volume for each measurement. The solutions were measured in a quartz microcuvette (Hellma; volume: 130 μL; thickness: 3 × 3 mm).

2.2. Instrumentation.

2.2.1. Raman Setup. The Raman measurements were performed with a LabRam HR 800 spectrometer from Horiba Jobin-Yvon. The system is optimized for UV excitation at 244 nm. This excitation line was generated by an argon−ion laser (Coherent Innova 300C MotoFred). The 488 nm laser line was intracavity frequency doubled through a BBO crystal. The nanoparticle samples placed in a microcuvette were illuminated via a microscope (Olympus BX 41) equipped with a 15× magnification objective (OFR). The Raman scattered light was collected with the same microscope objective in a 180°-backscattering geometry. The inelastic scattered Raman light was dispersed by a monochromator equipped with a 2400 L/mm grating. The resulting Raman photons were detected with a nitrogen-cooled CCD (Symphony Horiba Jobin-Yvon). The laser power at the laser head was 35 mW and on the sample 700 μW. The achieved spectral resolution with this setup was 5 cm^{-1}. The SER spectra of the analyte were obtained via time scans of 25 × 30 s. For the reference measurements, that is,

without addition of the analyte or colloids, respectively, time scans of 5 × 30 s were recorded.

2.2.2. UV−vis Absorption Spectroscopy. The UV−vis measurements were carried out with a Cary 5000 UV−vis absorption spectrometer from Varian. All samples were observed with a fiber-optical microcell (TrayCell, Hellma) to minimize the required sample volume for the colloid solutions. UV−vis absorption spectra in the range of 190−1000 nm were recorded from a 0.001 M aqueous solution of melamine and all colloid solutions. For the measurements in each case, 7 μL of the solution was used.

2.2.3. Scanning Electron Microscope (SEM) and Transmission Electron Miroscope (TEM). For SEM analysis, the scanning electron microscope JSM 6300F (JEOL) was used. Samples were prepared by dropping 2 μL of the colloid solution on a carbon pad. The droplets were dried at room temperature. The images were recorded with 5−10 kV using the secondary electron contrast.

For the very small colloids, the Ag prisms and Pd colloids, TEM images were recorded by using a Zeiss DSM 960 (Jena, Germany) transmission electron micorscope. A Formvar/carbon-coated TEM grid was used for the sample preparation. This grid was put in the nanoparticle solution overnight and subsequently air-dried under room temperature.

2.2.4. Analysis Techniques. The obtained spectra were analyzed with in-house written procedures with the help of the GnuR software package.[41] For every single SERS experiment, 25 measurements were carried out. The SER spectra shown in this publication are mean spectra calculated out of the 25 single SER spectra. For the reference measurements (i.e., without colloid or analyte), five spectra were recorded, and again the mean spectrum was calculated out of these five spectra. Before calculating the mean SER spectra, the spikes were removed from all single spectra. Peak heights and areas of the melamine marker band were determined by fitting it to a Gaussian profile (for every single spectrum). Means of the peak heights and areas were calculated afterward.

3. RESULTS AND DISCUSSION

3.1. Effect of the Particle Material. In this section, the pure colloids are characterized according to their size, shape, and SERS activity without the influence of an activation agent. To check if the metal particles allow for an electromagnetic SERS enhancement, UV−vis absorption spectra of all colloids were recorded to characterize the plasmon resonance. Figure 1 shows representative UV−vis spectra of some colloids, while in Table 1, the absorption maxima of all colloids can be found. Figure 1 also displays the absorption spectrum of melamine and the used SERS excitation wavelength of 244 nm as a vertical line. Figure 1 and Table 1 reveal that nearly all colloids show an absorption band in the UV. Under the assumption that a plasmonic resonance of the investigated colloids contributes to this UV absorption, almost all particles should be able to enhance a Raman signal via the electromagnetic SERS enhancement mechanism. The 20 nm Pd particles exhibit the largest absorption with a peak maximum at 247 nm, pretty close to the SERS excitation wavelength of 244 nm. The lowest absorption was detected for Pt 29 nm (Figure 1). In accordance with the UV−vis spectra, all used nanocolloids show SERS activity; that is, the melamine signal intensity increases once one of the colloids is added to the aqueous analyte solution. To characterize the size and shape of the used colloids, SEM and TEM images were recorded (see Figure 2 displaying some
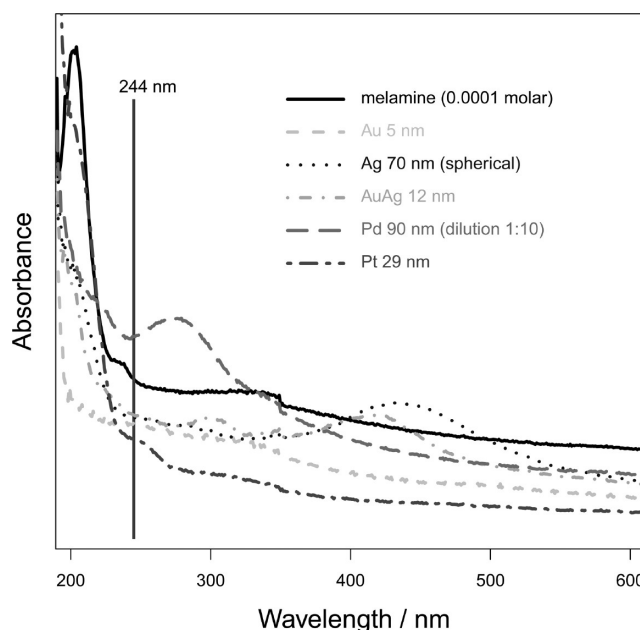

Figure 1. UV−vis spectra: solid line: 0.0001 M melamine solution; dashed line: 5 nm Au; dotted line: spherical 70 nm Ag; dotted−dashed line: 12 nm AuAg core−shell; long dashed line: 90 nm Pd in 1:10 aqueous dilution; two dashed line: 29 nm Pt; black bar: excitation wavelength 244 nm.

representative images): For example, Figure 2A shows that the Pt29 particles are homogeneous in size and nonaggregated. The TEM picture of a single Pd90 colloid shown in Figure 2B shows a pretty spherical shape with a diameter of around 90 nm. The SEM picture of the Ag70 colloid plotted in Figure 2C shows a homogeneous and nonaggregated distribution of these colloidal particles. Figure 2D displays a TEM image of the Au5 particles (black dots), which are well separated from each other and exhibit a uniform size distribution. The observed background originates from the TEM grid polymer. The AuAg12 core−shell nanoparticles shown in Figure 2E are of different morphology (that is, of triangular as well as pentagonal shapes), but of similar sizes. The SEM or TEM images of the other used particles can be found in the Supporting Information (Figures S1−S3).

To evaluate the different colloids with respect to their UV-SERS activity, we used melamine as a test analyte. Figure 3A, spectrum I, displays a UV-Raman spectrum of a 0.01 M aqueous melamine solution. The observed Raman bands might be resonantly enhanced (see UV−vis absorption spectrum of melamine and the 244 nm excitation laser line plotted in Figure 1). The Raman band at ca. 685 cm^{-1} with the highest intensity can be assigned to an in-plane deformation vibration of the triazine ring and the ring breathing 2 mode.[31] The Raman band at 990 cm^{-1} corresponds to a ring breathing mode and an in-plane deformation of the triazine ring of melamine.[31] To quantify the influence of the different colloids on the UV-(resonance)-Raman spectrum of melamine, the peak area of the most intense Raman band at 685 cm^{-1} determined by fitting it to a Gaussian profile has been utilized. The results of this band-fitting procedure (i.e., peak heights and peak areas) are summarized in Figure 4 and Table 2. In the following, we will start with discussing the influence of the inactivated colloids on the UV-Raman spectrum of melamine.
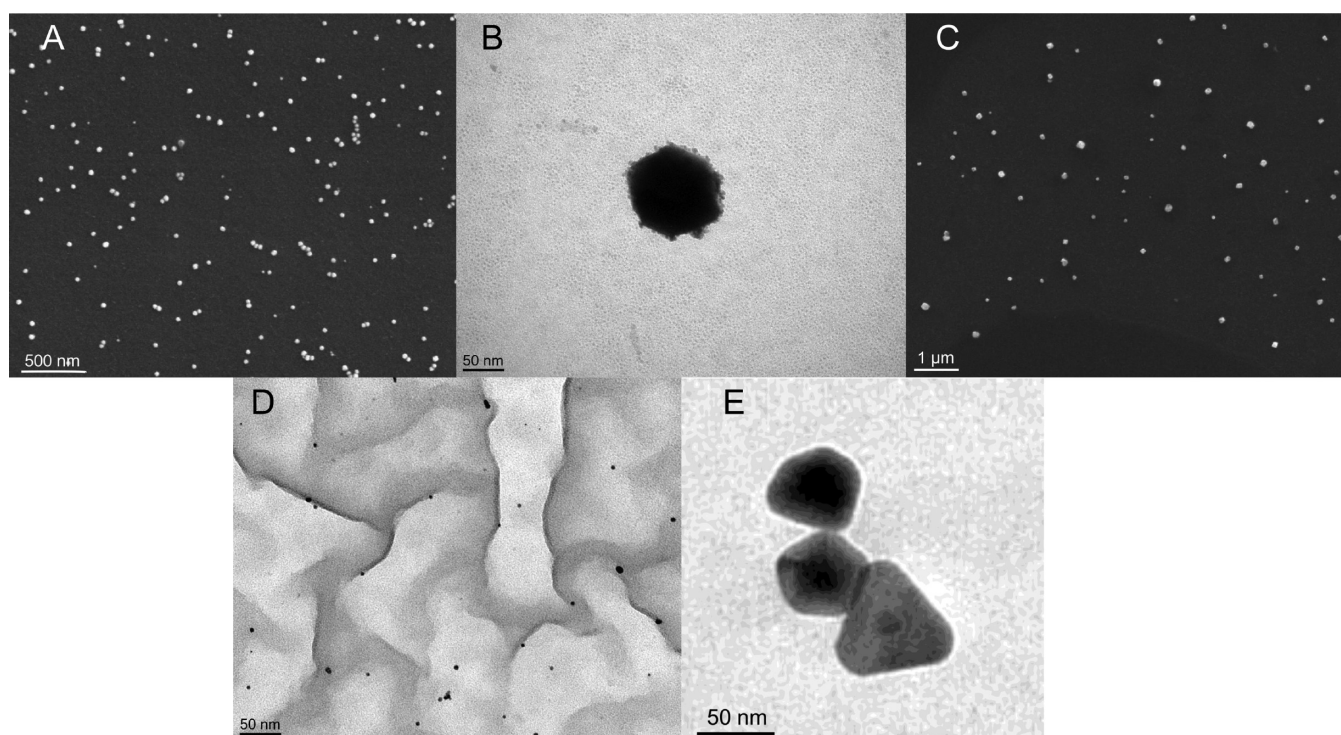
Figure 2. SEM and TEM images of the best acting nonaggregated colloids: (A) SEM image of Pt29; (B) TEM image of Pd90; (C) SEM image of Ag70; (D) TEM image of Au5; and (E) TEM image of AuAg12.
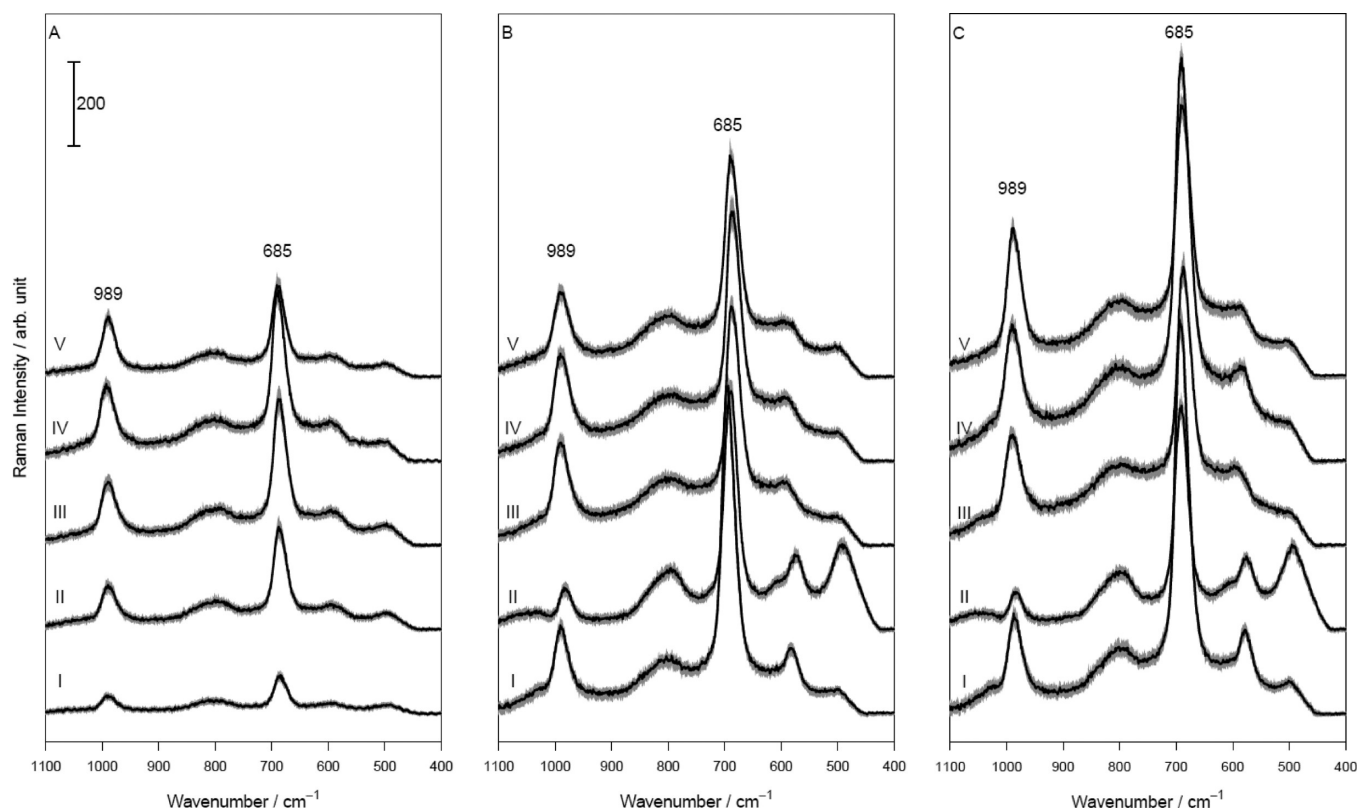
Figure 3. (A) Mean Raman spectra of pure melamine solution $c = 1 \times 10^{-2}$ M (I) and of melamine solution with KF (II), KCl (III), KBr (IV), and K_2SO_4 (V). (B) Nonactivated SER spectra of melamine $c = 5 \times 10^{-3}$ M with Pt29 (I), Pd90 (II), Ag70 (III), Au5 (IV), and AuAg12 (V). (C) Activated SER spectra of melamine with Pt107 + KCl (I), Pd90 + KCl (II), Ag23 + KCl (III), Au120 + KBr (IV), and AuAg12 + K_2SO_4 (V). Spectra shifted on the ordinate about 200 counts from each other; gray area around the spectra represents the standard deviation.

The most widely used metal for UV-SERS studies is platinum. Here, four different colloids with sizes of 29, 48, 73, and 107 nm are investigated. As can be seen in Table 1, all these Pt colloids absorb in the UV range (at around 200 nm).
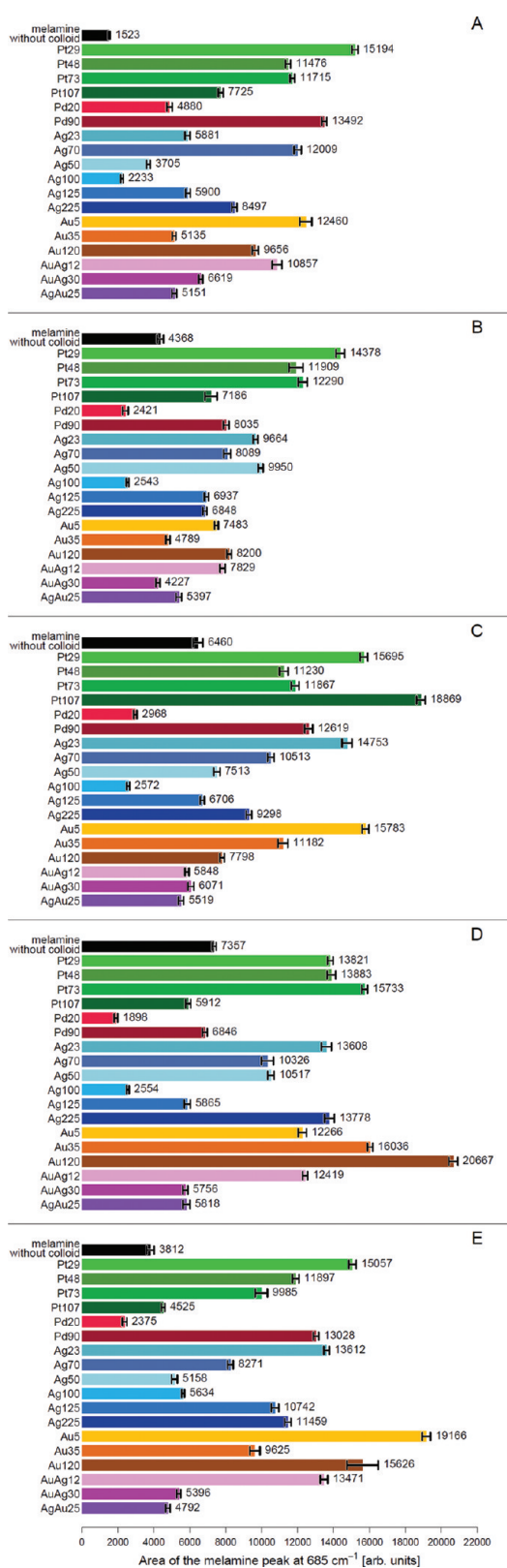
Figure 4. Bar plot of the peak area of the melamine band at around 685 cm^{-1} without activation (A), with KF (B), with KCl (C), with KBr (D), and with K$_2$SO$_4$ (E) always with all tested nanoparticles and without colloid (see the black bars); arrows correspond to the standard deviation.

Spectrum I in Figure 3B and Table 2 reveal that the Pt particles of 29 nm in diameter show the highest SERS activity. The Pt

particles of 48 and 73 nm in diameter show about the same SERS enhancement, whereas the largest Pt particles with a diameter of 107 nm lead to the lowest SERS activity (see Table 2). Like Pt, Pd can be also used for UV-SERS since Pd also has a plasmonic absorption in the UV (see Table 1). Here, we used two different Pd nanoparticles of 20 and 90 nm in diameter. The Pd particles with a diameter of 90 nm show a better SERS activity than the 20 nm diameter ones.

The two most commonly used SERS substrates for excitation wavelengths in the vis and NIR spectral range are Au and Ag nanoparticles. Here, we also exploited the efficiency of Au and Ag particles as UV-SERS substrates. As can be seen in Table 2, Au and Ag nanoparticles also show a good SERS activity for UV excitation. Here, it is particularly interesting to mention that, for silver, we also studied the influence of the particle shape. In doing so, we tested, besides the commonly used spherical Ag colloids, also Ag prisms of different sizes (see Table 1). It can be seen that the largest UV-SERS activity has been achieved for the spherical particles with a diameter of 70 nm (Figure 3B, spectrum III), followed by the largest triangular-shaped Ag colloids with an average edge length of 225 nm (see Table 2 and Figure 4A). Thus, also triangular particles lead to a significant UV-SERS activity. Overall, it could be shown that most of the tested Ag and Au nanoparticles exhibit a smaller UV-SERS activity than the Pt and Pd particles (see Table 2).

To combine the SERS properties of both silver and gold, we also checked for the UV-SERS acitivity of Au/Ag core−shell particles. Because Ag led to better results than Au, two AuAg core−shell particles are used; that is, the core is out of Au and the shell is a Ag one. Table 2 reveals that the core−shell particles with the smallest Au core (12 nm) exhibit the highest UV-SERS activity. This behavior is in good agreement with the one of pure Ag and Au colloids.

Overall, these studies with only the pure nanoparticles and no activation salt revealed as the best acting UV-SERS substrate Pt29, followed by Pd90. This behavior is in good agreement with the few studies[16−19,21] about UV-SERS, published in the last years. Interestingly, behind these two Pt and Pd particles, Ag70 and Au5, which are more typical for visible or NIR SERS excitation wavelengths, showed the best UV-SERS activity. The lowest SERS efficiency for 244 nm excitation was found for the Ag100 particle.

3.2. Effect of the Activation Agents. To investigate the influence of different activation agents, the four salts, KF (potassium fluoride), KCl (potassium chloride), KBr (potassium bromide), and K$_2$SO$_4$ (potassium sulfate), have been used. To quantify the influence of the different activation agents on the different colloidal particles, we used again the 685 cm^{-1} Raman mode of melamine. The resulting band heights and peak areas are analyzed and displayed in Figure 4 and Table 2.

Before we discuss the influence of the activation agents onto the SERS activity, we recorded Raman spectra of melamine in the presence of only the activation salts (i.e., no colloid) as a reference. The resulting mean Raman spectra shown in Figure 3A, spectra I−V, surprisingly reveal that the intensities of the two melamine peaks at 685 and 989 cm^{-1} are already influenced by the presence of the pure activation salts (the gray area around each spectrum illustrates the standard deviation). The black bars in Figure 4 summarize the influence of the pure activation salts on the peak area of the 685 cm^{-1} melamine Raman band: It can be seen that already the presence of an activation salt leads to an increased peak area as compared with the pure melamine Raman spectrum. The influence of the

6087

dx.doi.org/10.1021/jp211863y | J. Phys. Chem. C 2012, 116, 6083−6091

Table 2. Peak Heights and Areas for All Used Nanoparticles and Activation Agents

colloid	without activation		KF		KCl		KBr		K_2SO_4	
	area	height	area	height	area	height	area	height	area	height
Pd 20 nm	4880 ± 154.3	156 ± 5.2	2421 ± 155.3	69 ± 5.0	2968 ± 97.5	92 ± 3.8	1898 ± 98.0	50 ± 3.9	2375 ± 124.0	69 ± 5.3
Pd 90 nm	13 492 ± 140.3	471 ± 5.0	8035 ± 155.6	272 ± 7.4	12 619 ± 222.6	438 ± 10.3	6846 ± 135.0	233 ± 5.3	13 028 ± 153.5	458 ± 6.4
Pt 29 nm	15 194 ± 169.4	597 ± 8.4	14 378 ± 246.1	557 ± 7.8	15 695 ± 208.7	614 ± 7.1	13 821 ± 153.2	545 ± 9.6	15 057 ± 209.3	587 ± 6.8
Pt 48 nm	11 476 ± 141.7	470 ± 7.2	11 909 ± 386.8	478 ± 15.3	11 230 ± 244.6	461 ± 10.2	13 883 ± 240.3	562 ± 11.8	11 897 ± 181.2	487 ± 8.3
Pt 73 nm	11 715 ± 130.4	477 ± 5.9	12 290 ± 254.1	493 ± 11.8	11 867 ± 218.4	484 ± 9.2	15 733 ± 160.0	619 ± 7.9	9985 ± 338.5	407 ± 15.5
Pt 107 nm	7725 ± 135.6	308 ± 7.5	7186 ± 337.4	278 ± 13.5	18 869 ± 242.6	723 ± 11.5	5912 ± 142.7	244 ± 4.7	4525 ± 99.2	185 ± 4.0
Au 5 nm	12 460 ± 335.1	430 ± 12.2	7483 ± 104.6	261 ± 5.4	15 783 ± 189.6	524 ± 7.6	12 266 ± 234.3	401 ± 10.1	19 166 ± 234.6	557 ± 8.4
Au 35 nm	5135 ± 98.9	198 ± 3.7	4789 ± 112.7	185 ± 6.0	11 182 ± 275.7	406 ± 8.7	16 036 ± 150.8	563 ± 8.9	9625 ± 279.3	343 ± 11.1
Au 120 nm	9656 ± 1811.2	362 ± 5.3	8200 ± 126.4	305 ± 5.6	7798 ± 132.3	294 ± 5.2	20 667 ± 247.2	698 ± 7.8	15 626 ± 870.6	544 ± 33.5
Ag 23 nm	5881 ± 142.6	203 ± 5.0	9664 ± 130.7	323 ± 7.2	14 753 ± 279.2	471 ± 8.1	13 608 ± 277.9	445 ± 12.5	13 612 ± 155.1	453 ± 6.2
Ag 70 nm	12 009 ± 201.5	411 ± 2.4	8089 ± 194.8	286 ± 6.7	10 513 ± 182.6	651 ± 6.6	10 326 ± 330.5	349 ± 11.5	8271 ± 156.6	288 ± 6.1
Ag 50 nm	3705 ± 101.9	140 ± 3.8	9950 ± 130.3	339 ± 5.6	7513 ± 169.8	263 ± 5.7	10 517 ± 180.5	363 ± 5.9	5158 ± 157.9	188 ± 7.0
Ag 100 nm	2233 ± 73.1	88 ± 3.0	2543 ± 74.9	98 ± 3.0	2572 ± 82.9	99 ± 2.9	2554 ± 69.4	99 ± 2.5	5634 ± 79.3	210 ± 4.9
Ag 125 nm	5900 ± 129.2	219 ± 4.8	6937 ± 118.8	249 ± 3.7	6706 ± 113.8	242 ± 5.3	5865 ± 171.6	216 ± 7.0	10 742 ± 207.7	381 ± 5.3
Ag 225 nm	8497 ± 141	307 ± 4.4	6848 ± 109.1	241 ± 4.3	9298 ± 154.5	326 ± 5.7	13 778 ± 270.8	459 ± 8.2	11 459 ± 176.1	396 ± 6.5
AuAg 12 nm	10 857 ± 269.6	374 ± 9.7	7829 ± 148.6	273 ± 6.6	5848 ± 110.5	208 ± 4.0	12 419 ± 144.6	432 ± 6.9	13 471 ± 209.5	456 ± 8.1
AuAg 30 nm	6619 ± 110.2	230 ± 3.2	4227 ± 117.7	156 ± 5.3	6071 ± 163.6	209 ± 4.9	5756 ± 146.7	204 ± 5.6	5396 ± 110.1	194 ± 3.7
AgAu 25 nm	5151 ± 126.9	197 ± 6.5	5397 ± 155.2	191 ± 5.7	5519 ± 141.7	201 ± 5.5	5818 ± 189.6	205 ± 6.7	4792 ± 123.1	175 ± 4.4
melamine without colloid	1523 ± 49.3	63 ± 2.4	4368 ± 179.2	173 ± 5.6	6460 ± 279.3	251 ± 11.2	7357 ± 108.5	290 ± 4.9	3812 ± 204.7	154 ± 8.2

three potassium halogenides depends on the size of the halogenide anion: With increasing size of the anion, the melamine Raman intensity increases. Thus, the addition of KBr to the aqueous melamine solution causes the largest melamine Raman signal. This observed Raman signal increase upon addition of a salt might be due to solvation or changes in the pH value. Similar observations have been reported by Nagayama et al.,[42] who observed intensity changes within the Raman spectrum of D_2O upon addition of LiBr.

Figure 4B–E summarizes the results of the influence of an activation salt in combination with a metal colloid on the observed melamine Raman peak area at 685 cm^{-1}. As expected, the observed melamine peak area enhancements in the presence of the different SERS substrates are significantly larger than those obtained if only an activation salt is added to the melamine solution (see Figure 4). As shown in the preceding section, Pt29 and Pd90 showed the largest SERS enhancement without the presence of an activation agent. An activation of the Pt29 colloid with one of the tested activation agents led to no significant decrease or increase of the peak height and area of the investigated melamine marker band (see Table 2). However, the combination of Pd90 with the different activation agents resulted in lower SERS signals as compared with those of the inactivated colloid. In particular, for KF and KBr, the change for the worse is clearly visible (see Figure 4B,D). Nevertheless, the resulting peak heights and areas for the inactivated and activated Pd90 colloid are still significantly larger than those for the other tested Pd colloids with smaller diameters. Furthermore, no further increase of the melamine SERS signal was achieved by activation of the Ag70 colloid, which showed the third highest SERS activity without activation. The addition of KF and K_2SO_4 to Ag70 resulted even in a decreased SERS signal (Figure 4).

Within the group of the tested Au colloids, the 5 nm particles (Au5) led to the largest SERS signal if the colloids are not activated. However, the SERS efficiency achieved with this gold colloid (Au5) is largely influenced by an activation agent: For KBr activation, the resulting SERS signal is almost identical to that without activation, whereas the presence of KF decreases the SERS signal. However, if Au5 is activated with KCl, a significant increase in SERS activity is observed. The combination of Au5 with K_2SO_4 also results in a large increase in SERS activity as compared with that of the inactivated particle (Table 2). For the core–shell particle AuAg12, the melamine SERS signal can be increased upon addition of K_2SO_4 and KBr (compared with the inactivated particles). Otherwise, the melamine SERS signal using AuAg12 is decreased by activation with KF and KCl (Figure 4). For the group of the tested core–shell particles, AuAg12 is most efficient if it is used without activation.

Considering the different metals in combination with each activation agent, the following results can be found: Within the group of activated core–shell particles, AuAg12 in combination with K_2SO_4 as activation reagent remains the best acting colloid (Table 2 and Figure 3C, spectrum V). The inactivated best acting Au colloid Au5 is exceeded in efficiency by the combination of Au120 with KBr as activation agent (see Figure 4D). A similar behavior is found for the Ag colloids where the inactivated best acting Ag colloid Ag70 is less efficient than the combination of Ag23 with KCl activation (Table 2). For all possible combinations of Ag23 with one of the tested activation agents, a larger SERS activity of melamine

is achieved as compared with that of all activated Ag70 measurements (see Figure 4).

For the Pd colloids in combination with the different activation agents, the best SERS enhancement is found for the combination of Pd90 and K_2SO_4 (Figure 4E). Unfortunately, the improvement by activation as compared to the inactivated Pd90 is very low (Table 2). For most of the activated Pd colloids, the SERS signal decreases compared with that of the pure colloids (Figure 4). Figure 4C clearly shows that the activation of the largest Pt colloid (Pt107) with KCl leads to the largest peak area of the investigated melamine peak. However, this colloid shows only a good SERS efficiency with this activation agent. For all other activation salts and also in the case of the inactivated Pt particles, Pt107 leads in each case to the lowest peak heights and areas for all Pt particles (see Figure 4 and Table 2). For the combination of the Pt nanoparticles with K_2SO_4, an explicit trend can be observed: With an increasing size of the metallic nanoparticle, the SERS signal of melamine decreases. This tendency is also observed for the spherical Ag colloids, whereas an inverse behavior is observed for the group of the Ag prisms in combination with K_2SO_4. Here, the Ag prisms with increasing edge length show an increased SERS activity (see Figure 4E). These observations allow us to draw the conclusion that K_2SO_4 as an activation agent is very well suited for small spherical nanoparticles. For almost every group of metal particles, the smallest ones activated with K_2SO_4 showed the largest SERS activity. This trend that, for decreasing size of the metallic nanoparticle, the SERS enhancement increases can be also found for the Au colloids with KCl activation (see Figure 4C). The inverse behavior was observed for the Au colloids under activation with KBr. The largest Au colloid (Au120) activated with KBr shows the largest values of the peak area and height of the investigated melamine marker band (Figure 4D). This combination (Au120 + KBr) also leads to the best overall (all colloids and all activation agents) SERS enhancement of melamine under 244 nm excitation (see Figure 4 and Table 2). Thus, Au120 together with KBr is the best suited nanoparticle and activation agent combination for the detection of melamine in the UV (244 nm).

Overall, these studies showed that an activation agent is necessary to enhance the SERS signal. This can be best seen by comparing the SER spectrum of melamine using the Au120 colloid activated with KBr (the best combination of activator and nanoparticle) with the SER spectrum of melamine with Pt29 (best acting colloid without activation) (see Figure 3C, spectrum IV and Figure 3B, spectrum I). There is a significant increase in the peak height and area of the melamine marker band at around 685 cm^{-1} for the activated spectrum (Au120 + KBr).

4. CONCLUSION AND OUTLOOK

In this contribution, different metals and activation agents were tested in terms of their efficiency as UV-SERS substrates to detect melamine. To compare all the different substrates, the peak height and area of the in-plane deformation vibration of the triazine ring and the ring breathing 2 mode of melamine at around 685 cm^{-1},[31] determined by fitting it to a Gaussian profile, were used.

Au120 (spherical Au colloid with a diameter of 120 nm) activated with KBr emerged as the best combination of colloid and activation agent to detect melamine by means of UV-SERS using an excitation wavelength of 244 nm. This combination

6089

dx.doi.org/10.1021/jp211863y | *J. Phys. Chem. C* 2012, 116, 6083–6091

revealed the highest melamine SERS signal as compared to all other tested colloids and activation reagents. All of our studies showed that, for 244 nm excitation, no disturbing fluorescence background occurred, which makes UV-SER(R)S an efficient analytical tool for different research fields. Another interesting result was that Ag nanoparticles, which are typically used as SERS substrates with excitation wavelengths in the visible spectral region, also yield good results with UV excitation. All the used Ag samples, namely, the spherical colloids as well as the Ag prisms, show a significant UV-SERS enhancement. Furthermore, our studies revealed that the presence of an activation agent largely influences the UV-SERS activity. In other words, activation of the colloids led for some of the used particles to an increase in SERS activity, whereas for other particles, a decrease in activity could be observed. Unfortunately, for most cases, the influence of the activation agent was not predictable. Thus, the optimum combination of SERS-active metal and activation agent needs to be adjusted for every single application to obtain the best result. Overall, our results indicate that, for a perfect matching colloid and activation agent, the UV-SERS detection limit for illegal and toxic substances can be significantly downsized.

■ ASSOCIATED CONTENT

Ⓢ Supporting Information

SEM images of Pt48, Pt73, Pt107, Au35, and AuAg30 and TEM images of Au120, Pd20, Ag23, Ag225, Ag125, Ag100, Ag50, and AgAu25. This material is available free of charge via the Internet at http://pubs.acs.org.

■ AUTHOR INFORMATION

Corresponding Author

*E-mail: juergen.popp@uni-jena.de. Phone: +49(0)3641-206300.

Author Contributions

[⊥]This document is a collaborative effort of Evelyn Kämmer and Thomas Dörfer, and they contributed equally to the presented work.

Notes

The authors declare no competing financial interest.

■ ACKNOWLEDGMENTS

■ REFERENCES

(1) März, A.; Mönch, B.; Rösch, P.; Kiehntopf, M.; Henkel, T.; Popp, J. Detection of thiopurine methyltransferase activity in lysed red blood cells by means of lab-on-a-chip surface enhanced Raman spectroscopy (LOC-SERS). *Anal. Bioanal. Chem.* **2011**, *400*, 2755−2761.

(2) Xie, W.; Herrmann, C.; Kömpe, K.; Haase, M.; Schlücker, S. Synthesis of bifunctional Au/Pt/Au core/shell nanoraspberries for in situ SERS monitoring of platinum-catalyzed reactions. *J. Am. Chem. Soc.* **2011**, *133*, 19302−19305.

(3) Joseph, V.; Matschulat, A.; Polte, J.; Rolf, S.; Emmerling, F.; Kneipp, J. SERS enhancement of gold nanospheres of defined size. *J. Raman Spectrosc.* **2011**, *42*, 1736−1742.

(4) Hering, K.; Cialla, D.; Ackermann, K.; Dörfer, T.; Möller, R.; Schneidewind, H.; Mattheis, R.; Fritzsche, W.; Rösch, P.; Popp, J. SERS: A versatile tool in chemical and biochemical diagnostics. *Anal. Bioanal. Chem.* **2008**, *390*, 113−124.

(5) Blackie, E.; Le Ru, E. C.; Meyer, M.; Timmer, M.; Burkett, B.; Northcote, P.; Etchegoin, P. G. Bi-analyte SERS with isotopically edited dyes. *Phys. Chem. Chem. Phys.* **2008**, *10*, 4147−4153.

(6) Schmitt, M.; Popp, J. Raman spectroscopy at the beginning of the twenty-first century. *J. Raman Spectrosc.* **2006**, *37*, 20−28.

(7) Petschulat, J.; Cialla, D.; Janunts, N.; Rockstuhl, C.; Hübner, U.; Möller, R.; Schneidewind, H.; Mattheis, R.; Popp, J.; Tünnermann, A.; et al. Doubly resonant optical nanoantenna arrays for polarization resolved measurements of surface-enhanced Raman scattering. *Optics Express* **2010**, *18*, 4184−4197.

(8) Cialla, D.; Petschulat, J.; Hübner, U.; Schneidewind, H.; Zeisberger, M.; Mattheis, R.; Pertsch, T.; Schmitt, M.; Möller, R.; Popp, J. Investigation on the second part of the electromagnetic SERS enhancement and resulting fabrication strategies of anisotropic plasmonic arrays. *ChemPhysChem* **2010**, *11*, 1918−1924.

(9) Tarcea, N.; Harz, M.; Rösch, P.; Frosch, T.; Schmitt, M.; Thiele, H.; Hochleitner, R.; Popp, J. UV Raman spectroscopy-A technique for biological and mineralogical in situ planetary studies. *Spectrochim. Acta, Part A* **2007**, *68A*, 1029−1035.

(10) Wen, R.; Fang, Y. Surface Raman scattering studies on the adsorption of *p*-hydroxybenzoic acid at Au electrodes with ultraviolet excitation. *J. Electroanal. Chem.* **2005**, *576*, 237−242.

(11) Walter, A.; Reinicke, M.; Bocklitz, T.; Schumacher, W.; Rösch, P.; Kothe, E.; Popp, J. Raman spectroscopic detection of physiology changes in plasmid-bearing *Escherichia coli* with and without antibiotic treatment. *Anal. Bioanal. Chem.* **2011**, *400*, 2763−2773.

(12) Wang, P.; Wu, G. Ultraviolet laser excited surface enhanced Raman scattering of thiocyanate ion on the Au electrode. *Chem. Phys. Lett.* **2004**, *385*, 96−100.

(13) Wang, J. W.; Wang, W. N.; Fang, Y. Surface-enhanced Raman scattering studies on the adsorption of *p*-nitrobenzoic acid at Au electrode under different potential with ultraviolet excitation. *Vib. Spectrosc.* **2006**, *40*, 197−201.

(14) Ren, B.; Lin, X.-F.; Yang, Z.-L.; Liu, G.-K.; Aroca, R. F.; Mao, B.-W.; Tian, Z.-Q. Surface-enhanced Raman scattering in the ultraviolet spectral region: UV-SERS on rhodium and ruthenium electrodes. *J. Am. Chem. Soc.* **2003**, *125*, 9598−9599.

(15) Hao, Y.; Fang, Y. Ultraviolet Raman study of thymine on the Au electrode. *Spectrochim. Acta, Part A* **2007**, *68A*, 778−782.

(16) Cui, L.; Wang, A.; Wu, D.-Y.; Ren, B.; Tian, Z.-Q. Shaping and shelling Pt and Pd nanoparticles for ultraviolet laser excited surface-enhanced Raman scattering. *J. Phys. Chem. C* **2008**, *112*, 17618−17624.

(17) Hu, J.-W.; Li, J.-F.; Ren, B.; Wu, D.-Y.; Sun, S.-G.; Tian, Z.-Q. Palladium-coated gold nanoparticles with a controlled shell thickness used as surface-enhanced Raman scattering substrate. *J. Phys. Chem. C* **2007**, *111*, 1105−1112.

(18) Cui, L.; Mahajan, S.; Cole, R. M.; Soares, B.; Bartlett, P. N.; Baumberg, J. J.; Hayward, I. P.; Ren, B.; Russell, A. E.; Tian, Z. Q. UV SERS at well ordered Pd sphere segment void (SSV) nanostructures. *Phys. Chem. Chem. Phys.* **2009**, *11*, 1023−1026.

(19) Borodko, Y.; Habas, S. E.; Koebel, M.; Yang, P.; Frei, H.; Somorjai, G. A. Probing the interaction of poly(vinylpyrrolidone) with platinum nanocrystals by UV-Raman and FTIR. *J. Phys. Chem. B* **2006**, *110*, 23052−23059.

(20) Dörfer, T.; Schmitt, M.; Popp, J. Deep-UV surface-enhanced Raman scattering. *J. Raman Spectrosc.* **2007**, *38*, 1379−1382.

(21) Lin, X.-F.; Ren, B.; Yang, Z.-L.; Liu, G.-K.; Tian, Z.-Q. Surface-enhanced Raman spectroscopy with ultraviolet excitation. *J. Raman Spectrosc.* **2005**, *36*, 606−612.

(22) Ding, L.-P.; Fang, Y. The study of resonance Raman scattering spectrum on the surface of Cu nanoparticles with ultraviolet excitation and density functional theory. *Spectrochim. Acta, Part A* **2007**, *67A*, 767−771.

6090

dx.doi.org/10.1021/jp211863y | *J. Phys. Chem. C* 2012, 116, 6083−6091

(23) Brown, C. A.; Jeong, K.-S.; Poppenga, R. H.; Puschner, B.; Miller, D. M.; Ellis, A. E.; Kang, K.-I.; Sum, S.; Cistola, A. M.; Brown, S. A. Outbreaks of renal failure associated with melamine and cyanuric acid in dogs and cats in 2004 and 2007. *J. Vet. Diagn. Invest.* **2007**, *19*, 525−531.

(24) Chan, E. Y. Y.; Griffiths, S. M.; Chan, C. W. Public-health risks of melamine in milk products. *Lancet* **2008**, *372*, 1444−1445.

(25) Thompson, M.; Owen, L.; Wilkinson, K.; Wood, R.; Damant, A. A comparison of the Kjeldahl and Dumas methods for the determination of protein in foods, using data from a proficiency testing scheme. *Analyst (Cambridge, U.K.)* **2002**, *127*, 1666−1668.

(26) Guan, N.; Fan, Q.; Ding, J.; Zhao, Y.; Lu, J.; Ai, Y.; Xu, G.; Zhu, S.; Yao, C.; Jiang, L.; Miao, J.; Zhang, H.; Zhao, D.; Liu, X.; Yao, Y. Melamine-contaminated powdered formula and urolithiasis in young children. *N. Engl. J. Med.* **2009**, *360*, 1067−1074.

(27) Lam, C.-W.; Lan, L.; Che, X.; Tam, S.; Wong, S. S.-Y.; Chen, Y.; Jin, J.; Tao, S.-H.; Tang, X.-M.; Yuen, K.-Y.; Tam, P. K.-H. Diagnosis and spectrum of melamine-related renal disease: Plausible mechanism of stone formation in humans. *Clin. Chim. Acta* **2009**, *402*, 150−155.

(28) Sun, N.; Shen, Y.; He, L.-j. Histopathological features of kidney after acute renal failure from melamine. *N. Engl. J. Med.* **2010**, *362*, 662−664.

(29) Lutter, P.; Savoy-Perroud, M.-C.; Campos-Gimenez, E.; Meyer, L.; Goldmann, T.; Bertholet, M.-C.; Mottier, P.; Desmarchelier, A.; Monard, F.; Perrin, C.; Robert, F.; Delatour, T. Screening and confirmatory methods for the determination of melamine in cow's milk and milk-based powdered infant formula: Validation and proficiency-tests of ELISA, HPLC-UV, GC-MS and LC-MS/MS. *Food Control* **2011**, *22*, 903−913.

(30) Desmarchelier, A.; Cuadra, M. G.; Delatour, T.; Mottier, P. Simultaneous quantitative determination of melamine and cyanuric acid in cow's milk and milk-based infant formula by liquid chromatography-electrospray ionization tandem mass spectrometry. *J. Agric. Food Chem.* **2009**, *57*, 7186−7193.

(31) Koglin, E.; Kip, B. J.; Meier, R. J. Adsorption and displacement of melamine at the Ag/electrolyte interface probed by surface-enhanced Raman microprobe spectroscopy. *J. Phys. Chem.* **1996**, *100*, 5078−5089.

(32) Hu, H.; Wang, Z.; Pan, L.; Zhao, S.; Zhu, S. Ag-coated Fe_3O_4@SiO_2 three-ply composite microspheres: Synthesis, characterization, and application in detecting melamine with their surface-enhanced Raman scattering. *J. Phys. Chem. C* **2010**, *114*, 7738−7742.

(33) He, L.; Liu, Y.; Lin, M.; Awika, J.; Ledoux, D. R.; Li, H.; Mustapha, A. A new approach to measure melamine, cyanuric acid, and melamine cyanurate using surface enhanced Raman spectroscopy coupled with gold nanosubstrates. *Sens. Instrum. Food Qual. Saf.* **2008**, *2*, 66−71.

(34) Turkevich, J.; Stevenson, P. C.; Hillier, J. A study of the nucleation and growth processes in the synthesis of colloidal gold. *Discuss. Faraday Soc.* **1951**, *11*, 55−75.

(35) Frens, G. Controlled nucleation for the regulation of the particle size in monodisperse gold suspensions. *Nature* **1973**, *241*, 20−22.

(36) Aherne, D.; Ledwith, D. M.; Gara, M.; Kelly, J. M. Optical properties and growth aspects of silver nanoprisms produced by a highly reproducible and rapid synthesis at room temperature. *Adv. Funct. Mater.* **2008**, *18*, 2005−2016.

(37) Brust, M.; Fink, J.; Bethell, D.; Schiffrin, D. J.; Kiely, C. Synthesis and reactions of functionalized gold nanoparticles. *J. Chem. Soc., Chem. Commun.* **1995**, 1655−1656.

(38) Steinbrück, A.; Csaki, A.; Festag, G.; Fritzsche, W. Preparation and optical characterization of core−shell bimetal nanoparticles. *Plasmonics* **2006**, *1*, 79−85.

(39) Panigrahi, S.; Kundu, S.; Ghosh, S.; Nath, S.; Pal, T. General method of synthesis for metal nanoparticles. *J. Nanopart. Res.* **2004**, *6*, 411−414.

(40) Bigall, N. C.; Härtling, T.; Klose, M.; Simon, P.; Eng, L. M.; Eychmüller., A. Monodisperse platinum nanospheres with adjustable diameters from 10 to 100 nm: Synthesis and distinct optical properties. *Nano Lett.* **2008**, *8*, 4588−4592.

(41) *R: A Language and Environment for Statistical Computing*; R Foundation for Statistical Computing: Vienna, Austria, 2008. ISBN: 3-900051-07-0.

(42) Nagayama, H.; Hojo, M.; Ueda, T.; Nishimori, Y.; Okamura, M.; Daike, C. Effects of electrolytes on the configuration change of cobalt(II)-halide complexes in chloroform/water reverse micelle systems. *Anal. Sci.* **2001**, *17*, 1413−1420.